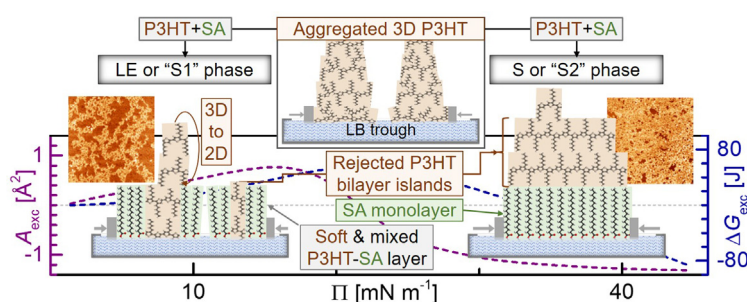


Stearic acid mediated growth of edge-on oriented bilayer poly (3-hexylthiophene) Langmuir films

Saugata Roy, Md Saifuddin, Subhankar Mandal, Satyajit Hazra *

Saha Institute of Nuclear Physics, HBNI, 1/AF Bidhannagar, Kolkata 700064, India

GRAPHICAL ABSTRACT



ARTICLE INFO

Article history:

Received 15 June 2021

Revised 5 August 2021

Accepted 12 August 2021

Available online 17 August 2021

Keywords:

Conjugated polymers
Fatty acid blending
Langmuir and LB films
X-ray reflectivity
Atomic force microscopy
3D to 2D transition
Edge-on orientation
Ordering and layering

ABSTRACT

The growth and structural evolution of stearic acid (SA) blended poly(3-hexylthiophene) [P3HT] Langmuir and Langmuir–Blodgett (LB) films were studied using complimentary surface and interface sensitive techniques to understand the possibility of ordering and layering of promising charge carrier mobility polymers, at the air–water interface and on the transferred solid substrate. SA-induced and subsequent compression-induced transitions in P3HT structure, from aggregated-3D to soft-2D and from in-plane mixed to unmixed layer, are evident at low and high pressures, respectively. The blending of SA molecules enhances the amphiphilic character of P3HT, which reduces the extent of the out-of-plane aggregation to form edge-on oriented (EO) bottom side-chain folded-bilayer (f-BL) islands (of size ~ 60 nm) within SA monolayer (ML), of commensurate thickness (~ 2.6 nm). Further compression, gradually rejects the less hydrophilic f-BL islands from the mixed layer to form EO P3HT BL islands (of coverage in-tune with starting composition) on top of SA ML. The formation of nearly covered P3HT(BL)/SA(ML) structured film on solid substrate is evident for the first time, which (even of limited P3HT thickness) has immense importance in the device properties, as the current in the bottom-gated organic thin-film transistors is known to travel only within few ML region near gate-dielectric.

© 2021 Elsevier Inc. All rights reserved.

1. Introduction

Conjugated polymers, due to their unusual but intriguing electrical and optical properties, enable advances in the fabrication of more efficient organic devices like light-emitting diodes, solar cells

and thin-film transistors (TFTs) [1–3]. Among the conjugated polymers, poly(3-alkylthiophene) [P3AT] is very much effective as an active layer in many opto-electronic devices due to its low cost, easier solution processing and substantial charge carrier mobility [4]. The alkyl side chain attached to P3AT thiophene ring makes it soluble in common organic solvents and thus promote simple solution processing for device fabrication [5–7]. In thin film, P3AT molecules form semicrystalline morphology, in which the

* Corresponding author.

E-mail address: satyajit.hazra@saha.ac.in (S. Hazra).

crystalline domains are separated by some amorphous regions. These crystalline domains, which are like lamellar structure, are formed due to a strong π - π interaction between the P3AT backbones [4,8]. The structural ordering and orientation of these crystalline domains, which do create a massive impact on the device performances, depend on various factors such as molecular weight [9], alkyl side chain-length [10], casting solvent [11,12], aging time [13], nature of the substrate [14] and to a great extent on the deposition techniques [15–18].

In recent years, a range of deposition techniques such as drop-casting, dip-coating and spin-coating have been used primarily to form P3AT thin films. Though such deposition techniques can produce the edge-on oriented (EO) ordering to some extent, it can not provide well-ordered EO structure, through layer-by-layer control, useful for the improvement of the charge carrier mobility. Langmuir–Blodgett (LB) and Langmuir–Schaefer (LS) deposition techniques [19–25], on the other hand, can offer excellent ways to fabricate a well-ordered structure through layer-by-layer transfer of the Langmuir monolayer (ML) from air–water interface to solid substrate. Although, well-ordered Langmuir MLs are easily formed for the amphiphilic molecules with hydrophilic head down and hydrophobic tail up at the air–water interface [25–28], the pure P3ATs usually agglomerate on the water surface due to their low amphiphilic nature and strong intermolecular (π - π) interaction [29]. Such agglomerated Langmuir film creates massive hindrance in the formation of well-ordered layer-by-layer structured P3AT film onto the solid substrate [30,31]. Thus controlling the structure of the Langmuir film of P3AT is of prime importance for the growth of well-ordered structured film onto the solid substrate through layer-by-layer transfer.

The structure of the P3HT Langmuir films can be controlled by tuning the nature of the solvent, the molecular weight and concentration of the polymer in the solution [32,33] and also by blending the amphiphilic fatty acid (FA) with P3AT [34–36]. The blending of FA is known to reduce the rigidity and enhance the amphiphilic character of P3AT, which in turn expected to improve their organization on the water surface. The possibility to improve or control the organization of P3AT, by FA blending, encouraged many to study its structures and properties [34–39]. Formation of P3AT and FA domain-mixed Langmuir ML was inferred directly from the surface pressure-area (Π - A) isotherm measurement and also indirectly from the optical, electrical and X-ray diffraction measurements of the multi-transferred LB films. Such mixed Langmuir film was referred as ML in terms of FA only and not in terms of P3AT (i.e. not necessary ML P3AT). In fact, no clear information about the number and structure of P3AT layer was available there. Further, the formation of rejected P3AT layer on top of FA ML at high pressure, in some cases, was also suggested from the isotherm measurement [34]. However, the information about the thickness and structure of that P3AT layer was not evident anywhere. Even, the presence of such separate P3AT layer was not clear from any other measurement. The lack of information about the actual structure and thickness of such P3AT in the mixed Langmuir film and detailed interaction between P3AT and FA are of real concern and limitation towards preparation of well-order layer structured P3AT films and thus need proper studies to improve the EO layered structures of P3AT, even of limited thickness, on solid substrates, as the current in the bottom-gated organic thin-film transistors is known to travel only within few ML region of the polymer film, near gate-dielectric [14].

In the present work, we have tried to overcome such concern by studying a model system, namely stearic acid (SA) blended poly(3-hexylthiophene) [P3HT], using complementary surface and interface sensitive techniques. P3HT was chosen, over other P3ATs, due to its promising field-effect mobility. The Π - A isotherm measurements [25–28] were used to predict the structures of the Lang-

muir films, while X-ray photoelectron spectroscopy (XPS) [40,41], X-ray reflectivity (XR) [42–44] and atomic force microscopy (AFM) [20,21] were used to understand the composition and structure of the singly transferred LB films. The XR essentially provides an electron density profile (EDP), i.e. in-plane average electron density as a function of depth, in high resolution, from which it is possible to estimate the film-structure [20,23]. The AFM provides a topographic information, i.e. surface morphology and depth-dependent surface coverage, from which it is also possible to estimate and/or verify the film-structure [22,13]. Indeed, formation of in-plane mixed LB films with SA of ML thickness and P3HT of commensurate thickness are evident at low pressure and layered LB films of rejected P3HT bilayer (BL) islands (of varying coverage) on top of SA ML are evident at high pressure for the first time from the complimentary XPS, XR and AFM measurements. The isotherm study further suggests that such structures are essentially formed at the air–water interface. An attempt has been made to understand such interesting structures in terms of interactions. Also, the possible implications of such near-covered BL-structured P3HT on ML SA, in the device properties, are discussed.

2. Experimental details

2.1. Preparation of P3HT–SA Langmuir and LB films

P3HT–SA solutions of fixed concentration ($c = 0.5 \text{ mg ml}^{-1}$) but varying composition (R , which is the weight-ratio of P3HT and SA) were prepared by mixing P3HT (average M_n : 54,000–75,000 and regioregularity $\geq 98\%$, Sigma-Aldrich) and/or SA (MW: 284.48 g mol^{-1} , Sigma-Aldrich) into chloroform (Merck) solvent and subsequent sonication for 10 min. P3HT–SA Langmuir and LB films were prepared using a LB trough (maximum area: 690 cm^2 , NIMA) placed in a clean environment. First the LB trough was thoroughly cleaned with water (Milli-Q, Millipore, resistivity 18.2 $\text{M}\Omega \text{ cm}$), then with isopropanol (Merck) and again with water to remove the contaminants. A Wilhelmy plate (a filter paper of dimension $10 \times 21 \text{ mm}^2$), dipped into the aqueous subphase, was used to measure the surface pressure. The P3HT–SA solution was then spread uniformly (drop-by-drop), using a micropipette, all over the trough and kept undisturbed (for about 10 min) for solvent evaporation and material suspension at air–water interface (at $24 \pm 1^\circ\text{C}$). Π - A isotherms of P3HT–SA Langmuir films were recorded at a constant compression speed (of $15 \text{ cm}^2 \text{ min}^{-1}$) by regulating two movable barriers.

Prior to the LB film deposition, Si(001) substrates were treated with RCA (Radio Corporation of America) cleaning procedure. At first Si substrates were sonicated in acetone and ethanol to remove some organic contaminants. After that Si wafers were transferred in a hot ($\sim 80^\circ\text{C}$) solution of ammonium hydroxide (NH_4OH , Merck, 25%), hydrogen peroxide (H_2O_2 , Merck, 30%), and water (H_2O) ($\text{NH}_4\text{OH}:\text{H}_2\text{O}_2:\text{H}_2\text{O} = 1:1:3$ by volume) for 10 min. Then the substrates were cleaned with water. This treatment results in the formation of OH-terminated Si surface (OH-Si) which is hydrophilic in nature [20,45]. LB films were deposited on OH-Si substrates by a single up-stroke through the subphase at a constant speed (of 2 mm min^{-1}). After deposition all the films were kept above the water subphase (for 5 min) for drying. Mixed P3HT–SA LB films were deposited for two compositions ($R = 1:1$ and $1:3$) and at two pressures ($\Pi = 14$ and 35 mN m^{-1}).

2.2. Characterization of P3HT–SA LB films

The XR measurements of the mixed P3HT–SA LB films were carried out using a X-ray diffractometer (Smartlab, Rigaku) [46] equipped with a copper source (sealed tube) followed by a Johans-

son Ge crystal and a parabolic multilayer mirror to obtain parallel beam of Cu $K_{\alpha 1}$ radiation (of wavelength 1.54 Å). The scattered beam was detected using a point (NaI scintillation) detector. Data were taken in specular condition, i.e., the incident angle is equal to the reflected angle (θ) and both are in a scattering plane [47–49]. Under such condition, there exists a nonvanishing wave-vector component, q_z , which is given by $(4\pi/\lambda) \sin \theta$ with a resolution of 0.0014 \AA^{-1} .

The XPS measurements of the mixed P3HT–SA LB films were carried out in an ultrahigh vacuum (UHV) multiprobe setup (Omicron Nanotechnology) at a base pressure of $\sim 2.0 \times 10^{-9}$ mbar, which was equipped with a monochromatic X-ray source (Al $K\alpha$ of energy 1486.6 eV) and a hemispherical energy analyzer (EA125) [50,51]. The corresponding spectrometer energy resolution was ~ 0.8 eV.

The detailed top surface morphologies of the mixed P3HT–SA LB films were mapped by an atomic force microscope (NanoScope IV, Veeco). Topographic images were collected using Al coated Si tip (radius of curvature ~ 10 nm) in a tapping mode (drive frequency ~ 285 kHz) to minimize tip-induced damage of the soft film. Scans of different sizes and in different portions of the sample were carried out to get statistically meaningful information about the topography. Processing and analysis of the AFM images were carried out using WSXM software [52].

3. Results and discussion

3.1. Π – A isotherms of P3HT–SA Langmuir films

Π – A isotherms of the P3HT–SA Langmuir films of different R -values are shown in Fig. 1, where A corresponds to mean area per molecule (for SA) and/or per monomer or thiophene unit (for P3HT). The different phases, namely liquid-expanded (LE), liquid-condensed (LC), their mixture (LE + LC) and solid-like (S), observed

in the isotherms are indicated [26–28]. The intermediate phases (namely LC and LC + LE) are almost absent in pure SA and P3HT isotherms. The presence of distinct LE and S phases are clear in the isotherms of pure SA and mixed Langmuir films but not in case of pure P3HT Langmuir film. Also the maximum pressure ($\Pi_{LE,max}$) up to which the LE phase exists in the SA Langmuir film ($\sim 26 \text{ mN m}^{-1}$) decreases in the mixed Langmuir films ($\sim 18 \text{ mN m}^{-1}$) and further in the P3HT Langmuir film ($\sim 10 \text{ mN m}^{-1}$). The absence of distinct LE phase and decrease of $\Pi_{LE,max}$ -value in the isotherm of pure P3HT indicate its rigid nature. The extrapolation of the solid-like branch of the isotherm to zero surface pressure, which provides the mean size or area (A_S) of a molecule and/or a thiophene unit, in the tightly packed condition [28], is indicated in Fig. 1. Corresponding mean area in the LE phase (A_{LE}) is also indicated. The A_S -value for the pure SA ($A_{S,SA}$) is found $\sim 21 \text{ \AA}^2$, which is consistent with the ML structure [39]. The A_S -value for the pure P3HT ($A_{S,P3HT}$) is found $\sim 4 \text{ \AA}^2$, which is very small compared to the area of a thiophene unit ($\sim 14.7 \text{ \AA}^2$), calculated according to the Corey–Pauling–Koltun (CPK) model [53,54], considering a close packed EO ML with all backbones are parallel but the thiophene rings are perpendicular to the air–water interface [55]. Such small value clearly indicates formation of out-of-plane aggregated or multilayered structures, deviating from a ML structure, at the air–water interface, due to the rigid nature of P3HT [29]. The variations of A_S and A_{LE} with SA mol% are plotted in the inset of Fig. 1, which show near-linear dependence. For A_S , the theoretical ($A_{S,th}$) and ideal ($A_{S,id}$) values are also included, apart from experimental ($A_{S,exp}$) values. The values of $A_{S,th}$ and $A_{S,id}$ have been estimated considering ideal mixing of P3HT and SA and their experimental ($A_{S,P3HT} \approx 4 \text{ \AA}^2$ and $A_{S,SA} \approx 21 \text{ \AA}^2$) and theoretical ($A_{S,P3HT} \approx 14.7 \text{ \AA}^2$ and $A_{S,SA} \approx 21 \text{ \AA}^2$) A_S -values, respectively. It is clear that, for the mixed P3HT–SA system, $A_{S,exp} \leq A_{S,th} \ll A_{S,id}$. This apparently indicates no decrease in the rigidity of P3HT (at least in the S phase) even after addition of amphiphilic SA, which is quite astonishing and thus needs proper understanding.

3.1.1. Viscoelastic property

The viscoelastic property or in-plane elasticity of the P3HT–SA Langmuir films can be investigated by calculating the compressional modulus, C_s^{-1} (reciprocal of monolayer compressibility C_s) [56,55], which is defined as

$$C_s^{-1} = -A \frac{d\Pi}{dA} \quad (1)$$

The variations of C_s^{-1} with A or Π for the P3HT–SA Langmuir films are represented in Fig. 2. It is evident that the values of C_s^{-1} at rela-

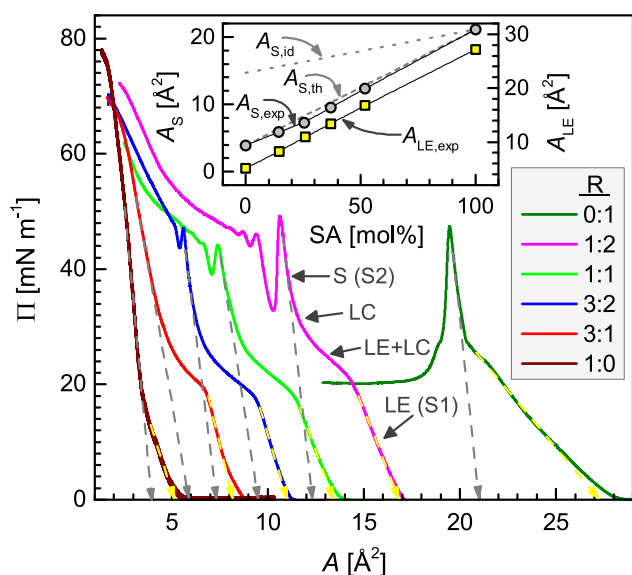


Fig. 1. Pressure–area (Π – A) isotherms of the P3HT–SA Langmuir films of different compositions (R), where A corresponds to mean area per molecule (for SA) and/or per monomer or thiophene unit (for P3HT). Different phases in an isotherm are indicated. Mean areas, A_S and A_{LE} , corresponding to the solid-like (S) and liquid expanded (LE) phases for each isotherm, are obtained from the intercepts of grey and yellow dashed lines to zero pressure. Inset: Variations of experimentally observed A_S (circle) and A_{LE} (square) with SA mol%. Considering ideal mixing of P3HT ($A_{S,P3HT}$) and SA ($A_{S,SA} \approx 21 \text{ \AA}^2$), the theoretical (where $A_{S,P3HT} \approx 14.7 \text{ \AA}^2$) and ideal (where $A_{S,P3HT} \approx 4 \text{ \AA}^2$) values of A_S , as calculated, are shown by dashed and dotted lines, respectively.

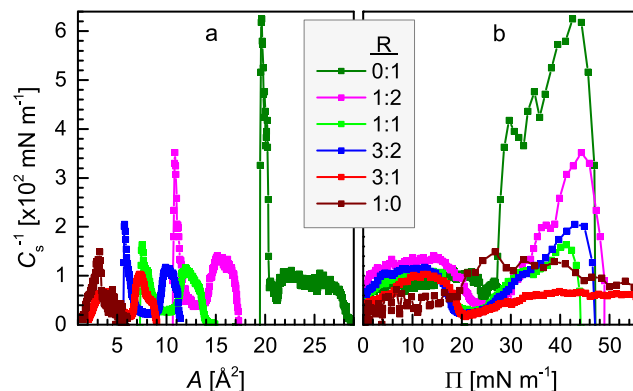


Fig. 2. Compressional modulus (C_s^{-1}) as a function of (a) mean area (A) and (b) surface pressure (Π) for the P3HT–SA Langmuir films of different compositions (R), as derived from isotherms.

tively large A -values (Fig. 2a) or at lower Π -values (Fig. 2b) are slightly higher for the pure SA and mixed P3HT-SA Langmuir films as compared to the pure P3HT Langmuir film. This indicates improvement of in-plane elasticity and stability in the mixed P3HT-SA Langmuir films over P3HT Langmuir films, in the LE phase, probably due to the formation of soft 2D mixed phase. A sharp drop in C_s^{-1} -value near $\Pi \approx 18 \text{ mN m}^{-1}$ is observed (in Fig. 2b) before reversing sign and increasing with Π within S phase. Such drop, which is consistent with the discontinuities in lateral packing at phase boundaries [57], indicates region of transition between two separate stable phases. Interestingly, not much improvement (rather deterioration for $R = 3:1$) in the in-plane elasticity, in comparison to the pure P3HT Langmuir film, is observed in the major portion of the S phase, consistent with the inference made in the previous section regarding rigidity. This clearly indicates that the structure of the Langmuir film in the S phase (where in-plane elasticity deteriorates) is different from that in the LE phase (where in-plane elasticity improves). Change in the structure from in-plane P3HT-SA mixed soft 2D to out-of-plane P3HT/SA mixed less soft 2D, as discussed later, is one possible way to interpret the observed deterioration in the in-plane elasticity.

3.1.2. Excess area

The insight about the interaction between P3HT and SA components in the mixed Langmuir films can be investigated, from a thermodynamic point of view, by calculating the excess area (A_{exc}) at a particular surface pressure. The value of A_{exc} is the deviation of the experimentally observed value (A_{exp}) from the theoretically expected value (A_{th}) [58]. The value of A_{th} can be calculated, considering ideal mixing of P3HT and SA, as

$$A_{\text{th}}(\Pi) = X_{\text{P3HT}}A_{\text{P3HT}}(\Pi) + X_{\text{SA}}A_{\text{SA}}(\Pi) \quad (2)$$

where, X_{P3HT} and X_{SA} are the mole fractions of P3HT and SA, respectively, in a mixture, while $A_{\text{P3HT}}(\Pi)$ and $A_{\text{SA}}(\Pi)$ are their mean molecular area at a certain pressure, Π , as obtained from the isotherms of pure P3HT and pure SA, respectively. Correspondingly, the value of A_{exc} can be expressed as

$$A_{\text{exc}}(\Pi) = A_{\text{exp}}(\Pi) - A_{\text{th}}(\Pi) \quad (3)$$

$A_{\text{exc}} = 0$ indicates that the binary components are immiscible and form an ideal mixing, this happens when there is no interaction between the components. Any deviation in the value of A_{exc} from zero indicates that the components are miscible and form a non-ideal mixing due to some interaction between the components. The variations of A_{exp} and A_{th} with Π are shown in Fig. 3a, while those of A_{exc} with Π are shown in Fig. 3b for the mixed P3HT-SA Langmuir films. The variation of A_{th} with Π is gradual, namely fast-decrease in the initial part and gradually slow-decrease with increasing Π . In comparison, the variation of A_{exp} with Π can be divided into three parts. In the first (LE phase) and last (S phase) parts the decrease is slow, while in-between, the decrease is fast, where crossover between A_{th} and A_{exp} takes place. Accordingly, a positive A_{exc} -value is observed in the first part and a negative A_{exc} -value is observed in the last part. This nature is similar for all the mixed P3HT-SA Langmuir films. However, the absolute value and the cross over position are different, especially for the film with $R = 1:2$. The positive A_{exc} -value indicates enhancement of mean molecular area, probably due to the presence of increased number of P3HT, apart from the SA molecules, in the vicinity of water surface. This is a signature of SA interaction mediated softening (or decrease in the out-of-plane stacking) of P3HT. The negative A_{exc} -value, on the other hand, indicates reduction in the mean molecular area due to some other interaction, which could be due to the rejection of such reduced out-of-plane stacked P3HT from the mixed layer, at the vicinity of water surface, and not due to the increase

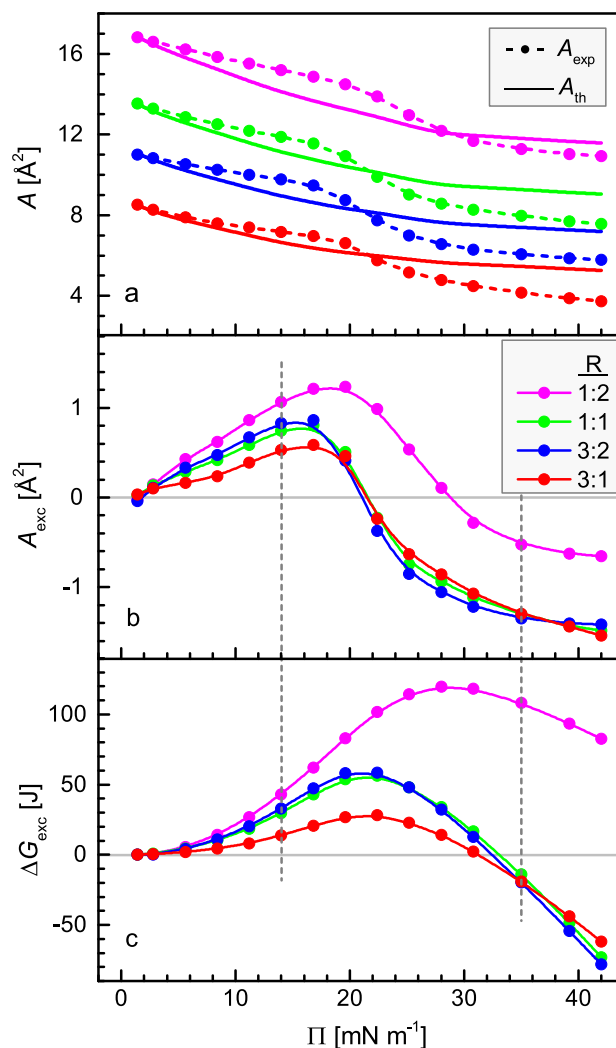


Fig. 3. Variations of (a) experimentally observed and theoretically calculated mean molecular areas (A_{exp} and A_{th}), (b) excess mean molecular area (A_{exc}) and (c) excess Gibbs free energy (ΔG_{exc}) with surface pressure (Π) for the P3HT-SA Langmuir layers of different compositions (R), as derived from isotherms. The deviations in the values of A_{exc} and ΔG_{exc} from zero at two pressures ($\Pi = 14$ and 35 mN m^{-1}) are indicated by dashed lines.

in the rigidity of P3HT, as inferred before (from inset of Fig. 1). The compression-decompression cycle study (see Figure S1 and related discussion of the Supporting Information) well supports this structural transition. The near saturation of the A_{exc} -value probably suggests nearly complete rejection of P3HT, thereby formation of a P3HT/SA structured Langmuir films, with top layer of rejected P3HT and bottom layer of amphiphilic SA molecules.

3.1.3. Excess Gibbs free energy

The strength and nature of interaction between P3HT and SA components in the mixed Langmuir films can be examined, from a thermodynamic point of view, by calculating the excess Gibbs free energy (ΔG_{exc}) [59]. The value of ΔG_{exc} is obtained by integrating A_{exc} over the surface pressure, as defined by

$$\Delta G_{\text{exc}}(\Pi) = N_A \int_{\Pi^*}^{\Pi} A_{\text{exc}} d\Pi \quad (4)$$

where N_A is the Avogadro number, Π^* corresponds to that of the gas-liquid expanded phase of the Π - A isotherm, which is normally taken as zero and Π is the upper limit of surface pressure at which

the ΔG_{exc} is to be calculated. For the ideally-mixed or immiscible systems $\Delta G_{\text{exc}} = 0$. The deviation of ΔG_{exc} from the ideal value ($\Delta G_{\text{exc}} = 0$) refers some kind of interaction between the components in the binary system. The large deviation indicates the strong interaction between the components. $\Delta G_{\text{exc}} > 0$ indicates repulsive interaction, while $\Delta G_{\text{exc}} < 0$ indicates attractive interaction. The variations of ΔG_{exc} with Π for different mixed P3HT–SA Langmuir films are shown in Fig. 3c. A small deviation in the ΔG_{exc} -value from the ideal value is observed, which indicates the presence of weak interaction between P3HT and SA molecules. The small positive ΔG_{exc} -value in the low- Π region (or LE phase) indicates a weak repulsive interaction (between in-plane dissimilar materials), which may arise due to the in-plane miscibility of P3HT and SA in the domain level but not in the molecular level. The small negative ΔG_{exc} -value in the high- Π region (or S phase) indicates a weak attractive interaction (between in-plane similar materials), which may arise within P3HT and SA molecules, present one above another in the P3HT/SA structured Langmuir films.

3.2. Structures of P3HT–SA LB films

The structures of the P3HT–SA LB films, which can validate some of the observations predicted from the thermodynamic point-of-view of the isotherms and provide further insight into the structures and growth of the P3HT–SA Langmuir films, are presented here. Four P3HT–SA LB films have been selected: two at different compositions ($R = 1:1$ and $3:1$) and two at different pressures ($\Pi = 14$ and 35 mN m^{-1} , corresponding to the LE phase (where A_{exc} and $\Delta G_{\text{exc}} > 0$) and S phase (where A_{exc} and $\Delta G_{\text{exc}} < 0$), respectively, as shown by the dashed lines in Fig. 3, which are well-separated from the low C_s^{-1} -value Π -region ($19\text{--}30 \text{ mN m}^{-1}$) and thus expected to provide better stability), to understand the effects of R and Π , and its derived thermodynamical parameters on the structures of the films.

3.2.1. XPS and chemical composition

The information about the chemical composition of the transferred LB film is useful and necessary in understanding its structure and thus estimated first using XPS technique. C 1s and S 2p core level spectra, recorded for the mixed P3HT–SA LB films of different starting compositions ($R = 1:1$ and $3:1$), are shown in Fig. 4. C 1s level (of binding energy 284.8 eV) was chosen as the reference level to calibrate the other core level spectra. The spectra were processed using PeakFit software, where a Shirley method was used to

subtract the background and the Gaussian–Lorentzian (GL) sum function was used to fit the XPS core-level spectra. Each C 1s spectrum, arising from the hydrocarbons (C) of both P3HT and SA molecules, was fitted with a single peak at around 284.8 eV, while S 2p spectrum, arising from the sulphur (S) atoms of P3HT, is overlapped with Si 2s plasmon loss peak. Overall S 2p spectrum was fitted with three distinct peaks: two peaks at $163.8 \pm 0.1 \text{ eV}$ and $165 \pm 0.1 \text{ eV}$ arising from S $2p_{3/2}$ and S $2p_{1/2}$ levels, respectively, and the third peak at $167.4 \pm 0.1 \text{ eV}$ corresponds to the Si 2s plasmon loss peak [60]. The ratio between the number of S and C atoms in the LB film, $(S/C)_{\text{LB}}$, is obtained by calculating the area under S $2p_{3/2}$ peak with respect to the area under the C 1s peak of the XPS spectra after considering the atomic sensitivity factor. For comparison, the ratio between the number of S and C atoms in the Langmuir film, $(S/C)_{\text{L}}$, is also calculated considering the starting composition, R . The values of $(S/C)_{\text{LB}}$ and $(S/C)_{\text{L}}$ for different R -values are tabulated in Table 1. $(S/C)_{\text{LB}}$ -values are in agreement (within 15%) with $(S/C)_{\text{L}}$ -values, which indicate that the starting compositions almost retain in the LB films. Over estimation of $(S/C)_{\text{LB}}$ -value probably signifies and justifies the presence of P3HT towards the upper-side of the film, as predicted from the isotherm.

3.2.2. XR and electron density profile

XR profiles of the P3HT–SA LB films of two compositions ($R = 1:1$ and $3:1$) deposited at two pressures ($\Pi = 14$ and 35 mN m^{-1}) are depicted in Figs. 5 and 6. Evolution of XR profile with Π is evident, namely a single broad peak or Kiessig fringe within $q_z \approx 0.15$ and 0.39 \AA^{-1} (with $\Delta q_z \approx 0.24 \text{ \AA}^{-1}$) at low Π -values becomes double peak (with $2\Delta q_z \approx 0.24 \text{ \AA}^{-1}$) at high Π -values, which indicates the increase in the film-thickness ($D = 2\pi/\Delta q_z$, from $\sim 2.6 \text{ nm}$ to $\sim 5.2 \text{ nm}$) with the increase in surface pressure. A slight evolution of XR profile with R is also evident, namely smearing of the single broad peak and enhancement in the second peak of the double peak (with change in the R -value from $1:1$ to $3:1$), which probably arise due to the change in the coverage, in general, and layered structure, in particular, of the film with composition.

In order to get the proper information about the structure of the films, the XR data were analyzed quantitatively using matrix method [43,44] after incorporating roughness at each interface [48]. For the analysis, each film was divided into a number of layers, of different thickness and electron density (ρ), after incorporating an interfacial oxide layer above the substrate. An instrumental resolution in the form of a Gaussian function and a constant background were also included at the time of data analysis [13]. It can be noted that a single layer of thickness $\sim 2.6 \text{ nm}$ was unable to reproduce the measured low Π -value XR data and a BL of thickness $\sim 5.2 \text{ nm}$ was unable to reproduce the measured high Π -value XR data (see Figures S2 and S3 of the Supporting Information). Accordingly, further layers, in commensurate with the structural prediction from the thermodynamic point-of-view of the isotherm, were added to reproduce the XR profiles (see Figures S1 and S2 of the Supporting Information). The best fit XR profiles thus obtained are shown in Figs. 5 and 6 and the corresponding EDPs are presented in the insets.

The EDPs along with the information of the compositions can well represent the structures of the films, as shown schematically in the insets of Figs. 5 and 6. The high density layer of thickness 2.6 nm , in the EDPs of the low Π -value films, is associated to the highly covered mixed-layer of SA and P3HT, where hydrophilic head of ML structured SA and less hydrophobic backbone of bottom side-chain folded BL (f-BL) structured P3HT are attached to the substrate. The subsequent low density high roughness layer is due to the presence of low-covered EO ML and BL structured P3HT on top. The coverage of such top structure, however, increases to some extent as the R -value changes from $1:1$ to

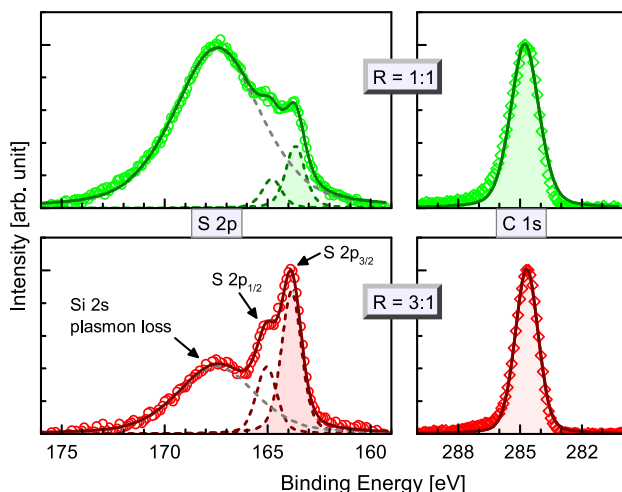


Fig. 4. S 2p and C 1s core level spectra for the mixed P3HT–SA LB films of different compositions (R). Each S 2p spectrum is the convolution of three peaks, as indicated.

Table 1

Parameters such as the ratio of sulphur and carbon atoms, $(S/C)_{LB}$, in the LB films (obtained from the XPS analysis) and $(S/C)_L$, in the Langmuir films (obtained considering the starting composition), the excess area (A_{exc}), the excess Gibbs free energy (ΔG_{exc}), the structure and composition of bottom layer, and the major structure of top P3HT layer for the P3HT–SA Langmuir and LB films of different pressures (Π) and compositions (R).

R	$(S/C)_{LB}$	$(S/C)_L$	Phase	Π [mN m ⁻¹]	A_{exc} [Å ²]	ΔG_{exc} [J]	Structure & composition of bottom layer	Major structure of top P3HT layer
1:1	0.054	0.049	LE or S1	14	0.7	30	ML SA + f – BL P3HT	ML (of <i>l</i> -C)
			S or S2	35	-1.3	-13	ML SA	BL (of <i>m</i> -C)
3:1	0.087	0.077	LE or S1	14	0.5	14	ML SA + f – BL P3HT	ML + BL (of <i>m</i> -C)
			S or S2	35	-1.3	-19	ML SA	BL (of <i>h</i> -C)

where ML: monolayer, BL: bilayer, f-BL: folded BL, *l*-C: low coverage, *m*-C: medium coverage and *h*-C: high coverage.

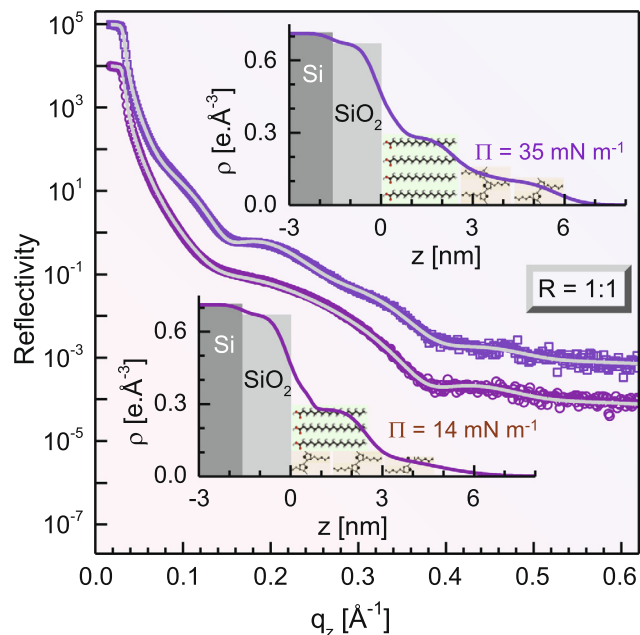


Fig. 5. XR data (symbols) and analyzed curves (solid lines) of P3HT–SA LB films of a fixed composition ($R = 1:1$) deposited at two different pressures (Π). Curves are shifted vertically for clarity. Insets: corresponding EDPs, indicating possible structures.

due to the increase in the P3HT content. It can be noted that the increase in the coverage of the top structure, in the $R = 3:1$ film, decreases the density contrast near $z = 2.6$ nm, which in turn smears the XR profile as observed. On the other hand, high density first layer of thickness 2.5 nm on top of the substrate, in the EDPs of the high Π -value films, can be associated to a hydrophilic head attached fully covered SA ML. Relatively low density next layer is due to the presence of EO BL structured P3HT. The coverage of such EO BL structure increases to a great extent as the R -value changes from 1:1 to 3:1 to form a near fully covered EO P3HT BL on top of a fully covered SA ML. The increased coverage of EO P3HT BL gives rise to a Kiessig fringe (indicative of total film-thickness) convoluted pseudo-Bragg peak near $q_z = 0.35$ Å⁻¹ as evident in the corresponding XR profile. Such pseudo-Bragg peak is essentially appearing from EO layering of P3HT.

3.2.3. AFM and topography

So far, the structures of the LB films are predicted from the XR study. Although the structures predicted from such reciprocal space mapping are quite complete, nonetheless, it is useful and necessary to cross verify them with real space mapping information. Typical AFM images for the mixed P3HT–SA LB films deposited at two different R -values and at two different Π -values are shown

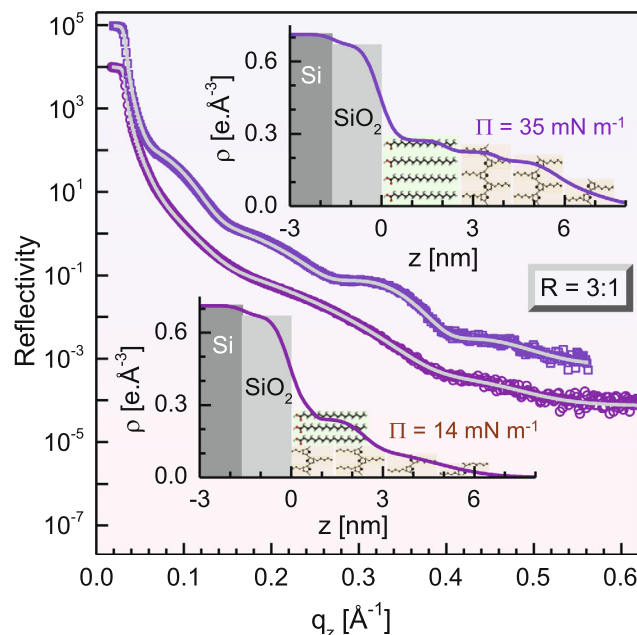


Fig. 6. XR data (symbols) and analyzed curves (solid lines) of P3HT–SA LB films of a fixed composition ($R = 3:1$) deposited at two different pressures (Π). Curves are shifted vertically for clarity. Insets: corresponding EDPs, indicating possible structures.

in Fig. 7. The network-like or nearly-packed structures, consisting of small domains, on top of a nearly covered layer is observed in all the AFM images. The presence of small domains is clear in the high resolution images. The average size of such domains (~ 60 nm, as evident from Figure S4 and related discussion of the Supporting Information) remains almost same for all the films, which closely resembles the polymerization length [13]. The transition from network-like structure to nearly-packed structure takes place with the increase of R -value, while the coverage of such structures increases with the increase of Π -values and almost covered structure is observed for the film with high R and Π values.

To get better insight about the film structure, the bearing area (BA) and the surface coverage (SC), as obtained from the AFM images, are plotted as a function of height (z) in Fig. 8. The increase in BA with z , for the film with low R and Π values, is initially fast then slow, which for the film with high R or Π values becomes relatively slow and then relatively fast and for the film with high R and Π values is initially slow and then fast. Two peaks are observed in all the SC profiles, however, their relative position and intensity are found to change with the R or Π values. In the low Π value films, the first peak near 2.5 nm, can be correlated with the near-fully-covered mixed layer of SA and P3HT (of thickness about

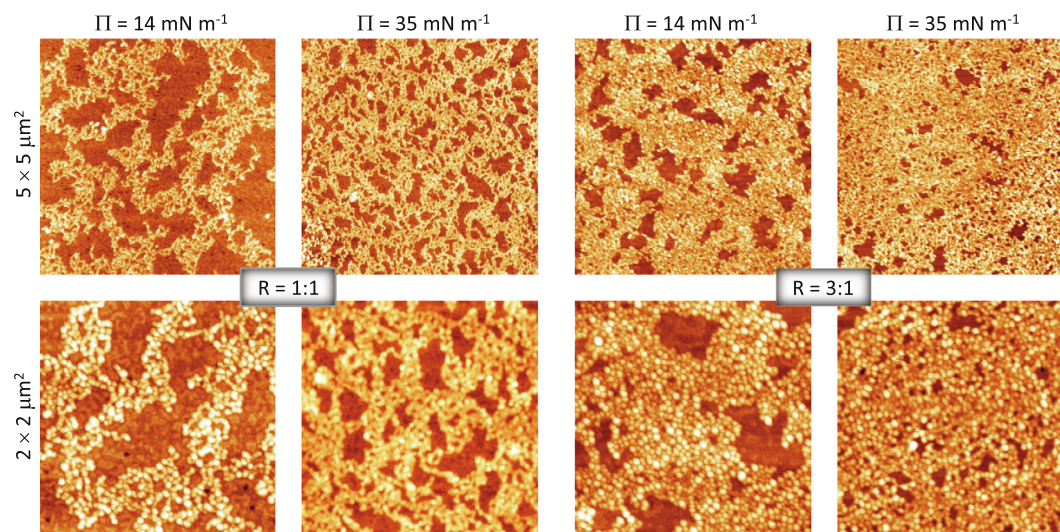


Fig. 7. AFM images in two different scan sizes for the mixed P3HT-SA LB films deposited at two different compositions (R) and at two different pressures (Π).

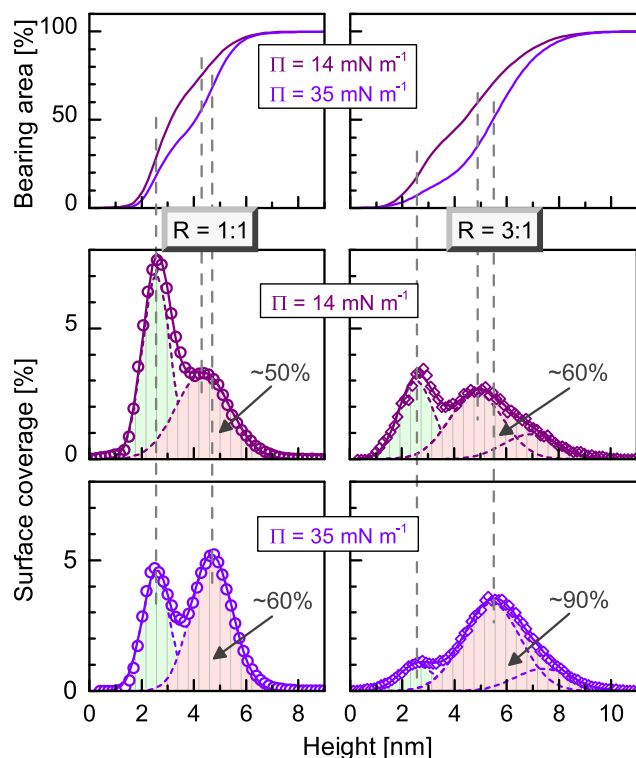


Fig. 8. Bearing area (solid lines), surface coverage (symbols) and Gaussian deconvoluted surface coverage (solid lines) as a function of height (obtained from AFM images) for the mixed P3HT-SA LB films deposited at two different compositions (R) and at two different pressures (Π). Integrated surface coverage (light orange), other than contribution from the first peak (light green), is indicated. (For interpretation of the references to color in this figure legend, the reader is referred to the web version of this article.)

2.5 nm), while the second peak near 4.3 or 4.9 nm, can be correlated with the partially-covered ML and BL mixed layer of EO P3HT on top. The increase in the thickness (from 1.8 to 2.4 nm) with increase in the R -value indicates increase in the ratio between BL and ML coverage (from 1:3 to 3:2) in the partially-covered EO P3HT layer, while the increase in the integrated coverage around the second peak (from $\sim 50\%$ to $\sim 60\%$) with increase in the R -value is mainly due to the presence of beyond BL structure (indi-

cated by deconvoluted third peak) in the partially-covered P3HT layer. In the high Π -value films, the first peak near 2.5 nm, can be correlated with the fully-covered ML of SA, while the second peak near 4.7 or 5.5 nm, can be correlated with the better covered EO P3HT BL. The increase in the integrated area around the second peak (from $\sim 60\%$ to $\sim 90\%$) with increase in the R -value suggests the overall increase in the coverage of the EO P3HT BL along with the presence of some beyond BL structure (indicated by deconvoluted third peak), while the decrease in the BL thickness (from 3.0 to 2.2 nm) with the decrease in the R -value indicates increase in the tilt angle (or deterioration in the EO ordering) of the P3HT BL probably due to the decrease in the compaction arising from less coverage. The structures of the mixed P3HT-SA LB films obtained here from the real space AFM images, though overestimate the coverage due to the tip-convolution and underestimate the height due to the image-flattening, are in agreement with those predicted from the reciprocal space XR data.

4. Overall structure and its implication

In conclusions, let us first represent the growth and overall structure of the P3HT-SA Langmuir films and then their possible implications in the device properties. The structures of the P3HT-SA Langmuir films can be modeled, by combining the complementary information (in Table 1) obtained from the isotherms and the structures of the LB films, as shown schematically in Fig. 9. The SA molecules, due to their amphiphilic nature, when spread on the water surface form loosely-packed (in LE phase) and densely-packed (in S phase) ML Langmuir films with hydrophilic head down and hydrophobic tail up at air-water interface (shown in Fig. 9a and b) [25–28]. The P3HTs, due to their strong π - π stacking interaction and low amphiphilicity, when spread on the water surface, form randomly stacked 3D aggregates (as $A \approx 4 \text{ \AA}^2 \ll 14.7 \text{ \AA}^2$) at the air-water interface [29], to minimize the polymer-water contact or interaction (the coverage of which increases little-bit with the barrier compression as shown in Fig. 9c and d).

The SA blended P3HT when spread on the water surface, the amphiphilic SA reduces the rigidity and enhances the amphiphilic character of P3HT, which in turn reduces the random 3D aggregation and promotes the EO 2D structures ($A_{exc} > 0$, to form in-plane mixed P3HT-SA layer) at the air-water interface as evident in the low pressure (see Fig. 9e). Such mixing is not in the molecular

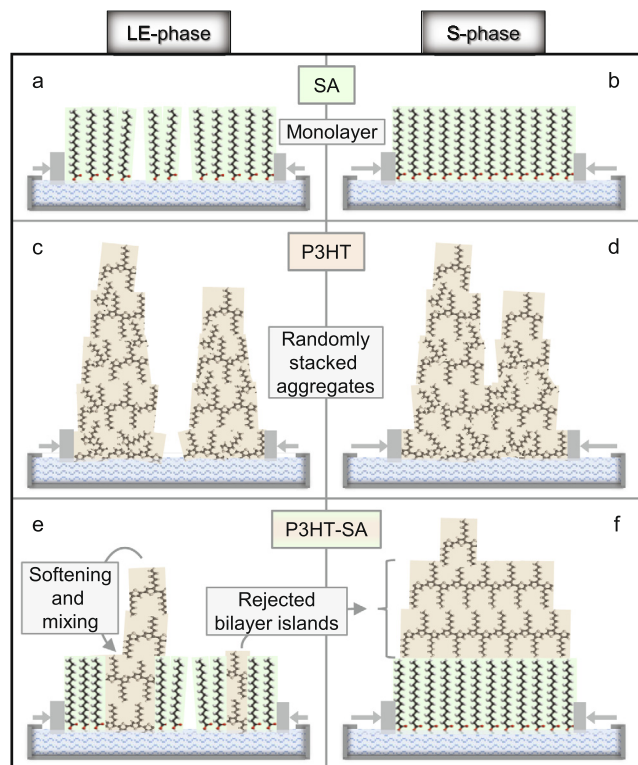


Fig. 9. Structural schematics of SA, P3HT and P3HT-SA Langmuir films (at air-water interface of LB trough) at the liquid-expanded (LE) and solid-like (S) phases, showing formation of (a) and (b) 2D (ML) structured SA Langmuir films, (c) and (d) 3D (aggregated multilayer) structured P3HT Langmuir films, and (e) soft in-plane mixed P3HT-SA Langmuir film at LE (or “S1”) phase and (f) rejected edge-on oriented P3HT BL islands on top of SA ML, i.e. P3HT/SA structured Langmuir film at S (or “S2”) phase.

level, rather in the domain level, where P3HT islands experience repulsion from the adjacent SA molecules, as evident from the thermodynamical parameters ($\Delta G_{exc} > 0$). The formation of EO domains or islands of P3HT can be understood by the presence of polymer (not monomer) back-bones and their π - π stacking. Thus the enhanced-amphiphilic character of P3HT does not weaken the π - π stacking interaction much rather reduces the extent of the out-of-plane interaction and aggregation to interact more with the water surface to form soft and stable 2D P3HT islands. Such reduction in the out-of-plane aggregation (as $A_{th} < A_{exp} < A_{id}$) seems to produce mostly EO f-BL islands (of height ~ 2.6 nm) rather than ML P3HT islands (of height ~ 1.6 nm). The hydrophobic side-chains of the EO BL P3HT islands, which come in contact with water, feel strong repulsion and thus folded to form EO f-BL P3HT islands of SA ML commensurate height. The ratio of P3HT islands and SA molecules and their packing, in the mixed layer, increases with composition and barrier-compression, respectively, within LE phase. It can be noted that not all P3HT aggregates are reduced to near BL structures as ML, BL and even TL-like structures of small coverage, on top of the mixed layer, are evident in the LB films.

On further barrier-compression, beyond LE phase, the less hydrophilic EO f-BL P3HT islands in the mixed layer, having in-plane repulsive interaction with SA molecules ($\Delta G_{exc} > 0$), gradually squeezed-out of the water surface to form EO BL P3HT islands (of height ~ 3.2 nm) on top of SA ML (of height ~ 2.5 nm) at S phase (shown in Fig. 9f). This indicates that, for the P3HT-SA mixed system, the said LE phase is actually a “mixed single-layer solid-like (S1)” phase, while the said S phase is actually an “unmixed two-

layer solid-like (S2)” phase. The squeezing out of the P3HT islands decreases the overall in-plane occupied area of the Langmuir film on the water surface (as evident from $A_{exc} < 0$) and creates attractive in-plane interaction within SA molecules and also within P3HT islands (as evident from $\Delta G_{exc} < 0$) to form a stable P3HT(BL)/SA (ML) structured Langmuir film, which can be transferred onto a solid substrate using LB technique, unlike inferred before [34–39]. The coverage of such EO BL P3HT islands on the top layer increases with barrier-compression and composition, however, their average size (~ 60 nm) remains unaltered. This indicates that domains of fixed average size are formed at the initial stages, through π - π stacking, when mixed solution was spread on the water surface. The average size of such domains seems to correlate more with the polymerization length [13]. It can be noted that though squeezing of P3HT and their better organization at high pressure have been proposed from isotherm and PM-IR-RAS studies [34,39] but no inference on their orientation and thickness have been made before.

The overall structural studies suggest SA-induced initial transition in P3HT structure, from aggregated 3D to soft 2D and barrier compression-induced subsequent transition in P3HT structure, from in-plane mixed to unmixed layer, which are quite interesting. Though, a single (SA-induced) transition is not expected to improve the in-plane electrical transport, as ordered 2D P3HT islands are dispersed in an insulating SA matrix at low pressure “S1” phase, the combination of (SA- and compression-induced) transitions is expected to promote the in-plane electrical transport, through layer of EO ordered 2D P3HT islands, at high pressure “S2” phase. Also, the formation of nearly covered P3HT(BL)/SA(ML) structured film on solid substrate through LB technique is evident for the first time. Such EO P3HT film, though has a limited thickness (namely BL), is of immense importance in the improvement of the in-plane charge carrier mobility and the device properties, as the current in the bottom-gated organic thin-film transistors is known to travel only within few ML region of the polymer film, near gate-dielectric [14].

It can be noted that the number and coverage of BL-structured P3HT, though quite high in the LB film, not all P3HT aggregates are found to reduce to near BL structures and thus can be further optimized (through 3D to 2D transition) by tuning the concentration [32,33] and fine tuning the ratio of P3HT and SA in the solution, which will be interesting to verify in future, for the improvement of the device properties. Additionally, it will be interesting to perform in-situ X-ray and neutron reflectivity [61,62,57] and grazing incidence diffraction (GID) measurements of the P3HT-SA Langmuir film at air-water interface, in future, to directly characterize and confirm the proposed out-of-plane and in-plane structures of the Langmuir film.

CRedit authorship contribution statement

Saugata Roy: Methodology, Investigation, Data curation, Formal analysis, Writing – original draft. **Md Saifuddin:** Formal analysis, Investigation. **Subhankar Mandal:** Data curation, Formal analysis. **Satyajit Hazra:** Conceptualization, Supervision, Visualization, Validation, Writing – review & editing.

Declaration of Competing Interest

The authors declare that they have no known competing financial interests or personal relationships that could have appeared to influence the work reported in this paper.

Acknowledgments

The authors thank Dr. Ramkrishna Dev Das and Mr. Goutam Sarkar for their help in XR and XPS measurements. Authors also like to acknowledge Prof. Mrinmay K Mukhopadhyay for providing the XR facility. M.S. acknowledges University Grant Commission (UGC), India and S.M. acknowledges Council of Scientific & Industrial Research (CSIR), India for providing research fellowships.

Appendix A. Supplementary material

Supplementary data associated with this article can be found, in the online version, at <https://doi.org/10.1016/j.jcis.2021.08.071>.

References

- J.H. Burroughes, D.D.C. Bradley, A.R. Brown, R.N. Marks, K. Mackay, R.H. Friend, P.L. Burns, A.B. Holmes, Light-emitting diodes based on conjugated polymers, *Nature* 347 (1990) 539–541.
- L. Qiu, W.H. Lee, X. Wang, J.S. Kim, J.A. Lim, D. Kwak, S. Lee, K. Cho, Organic thin-film transistors based on polythiophene nanowires embedded in insulating polymer, *Adv. Mater.* 21 (2009) 1349–1353.
- Y. Liang, Z. Xu, J. Xia, S.-T. Tsai, Y. Wu, G. Li, C. Ray, L. Yu, For the bright future—bulk heterojunction polymer solar cells with power conversion efficiency of 7.4%, *Adv. Mater.* 22 (2010) E135–E138.
- H. Sirringhaus, P.J. Brown, R.H. Friend, M.M. Nielsen, K. Bechgaard, B.M.W. Langeveld-Voss, A.J.H. Spiering, R.A.J. Janssen, E.W. Meijer, P. Herwig, D.M. de Leeuw, Two-dimensional charge transport in self-organized, high-mobility conjugated polymers, *Nature* 401 (1999) 685–688.
- K.-Y. Jen, G.G. Miller, R.L. Elsenbaumer, Highly conducting, soluble, and environmentally-stable poly(3-alkylthiophenes), *J. Chem. Soc., Chem. Commun.* (1986) 1346–1347.
- R.L. Elsenbaumer, K.Y. Jen, R. Oboodi, Processible and environmentally stable conducting polymers, *Synth. Met.* 15 (1986) 169–174.
- S. Hotta, S.D.D.V. Rughoputh, A.J. Heeger, F. Wudl, Spectroscopic studies of soluble poly(3-alkylthiophenes), *Macromolecules* 20 (1987) 212–215.
- I. Roy, S. Hazra, Poor solvent and thermal annealing induced ordered crystallites in poly(3-dodecylthiophene) films, *RSC Adv.* 5 (2015) 665–675.
- R.J. Kline, M.D. McGehee, E.N. Kadnikova, J. Liu, J.M.J. Fréchet, Controlling the field-effect mobility of regioregular polythiophene by changing the molecular weight, *Adv. Mater.* 15 (2003) 1519–1522.
- V. Causin, C. Marega, A. Marigo, L. Valentini, J.M. Kenny, Crystallization and melting behavior of poly(3-butylthiophene), poly(3-octylthiophene), and poly(3-dodecylthiophene), *Macromolecules* 38 (2005) 409–415.
- J.-F. Chang, B. Sun, D.W. Breiby, M.M. Nielsen, T.I. Sölling, M. Giles, I. McCulloch, H. Sirringhaus, Enhanced mobility of poly(3-hexylthiophene) transistors by spin-coating from high-boiling-point solvents, *Chem. Mater.* 16 (2004) 4772–4776.
- I. Roy, S. Hazra, Solvent dependent ordering of poly(3-dodecylthiophene) in thin films, *Soft Matter* 11 (2015) 3724–3732.
- M. Saifuddin, M. Mukhopadhyay, A. Biswas, L. Gigli, J.R. Plaisier, S. Hazra, Tuning the edge-on oriented ordering of solution-aged poly(3-hexylthiophene) thin films, *J. Mater. Chem. C* 8 (2020) 8804–8813.
- R.J. Kline, M.D. McGehee, M.F. Toney, Highly oriented crystals at the buried interface in polythiophene thin-film transistors, *Nat. Mater.* 5 (2006) 222–228.
- M. Brinkmann, J.C. Wittmann, Orientation of regioregular poly(3-hexylthiophene) by directional solidification: A simple method to reveal the semicrystalline structure of a conjugated polymer, *Adv. Mater.* 18 (2006) 860–863.
- A. Salleo, R.J. Kline, D.M. DeLongchamp, M.L. Chabiny, Microstructural characterization and charge transport in thin films of conjugated polymers, *Adv. Mater.* 22 (2010) 3812–3838.
- T. Salamal Shabi, S. Grigorian, M. Brinkmann, U. Pietsch, N. Koenen, N. Kayunkid, U. Scherf, Enhancement in crystallinity of poly(3-hexylthiophene) thin films prepared by low-temperature drop casting, *J. Appl. Polym. Sci.* 125 (2012) 2335–2341.
- M. Ito, Y. Yamashita, Y. Tsuneda, T. Mori, J. Takeya, S. Watanabe, K. Ariga, 100°C–Langmuir–Blodgett method for fabricating highly oriented, ultrathin films of polymeric semiconductors, *ACS Appl. Mater. Interfaces* 12 (2020) 56522–56529.
- J.K. Basu, S. Hazra, M.K. Sanyal, Growth mechanism of Langmuir–Blodgett films, *Phys. Rev. Lett.* 82 (1999) 4675–4678.
- J.K. Bal, S. Kundu, S. Hazra, Growth and stability of Langmuir–Blodgett films on OH-, H-, or Br-terminated Si(001), *Phys. Rev. B* 81 (2010) 045404.
- M. Mukhopadhyay, S. Hazra, Growth of thiol-coated Au-nanoparticle Langmuir monolayers through a 2D-network of disk-like islands, *RSC Adv.* 6 (2016) 12326–12336.
- M. Mukhopadhyay, S. Hazra, Interfacial and thermal energy driven growth and evolution of Langmuir–Schaefer monolayers of Au-nanoparticles, *Phys. Chem. Chem. Phys.* 20 (2018) 1051–1062.
- M. Mukhopadhyay, S. Hazra, Evolution of ligand-capped nanoparticle multilayers toward a near unique thickness, *Soft Matter* 15 (2019) 1869–1878.
- K. Ariga, Don't forget Langmuir–Blodgett films 2020: Interfacial nanoarchitectonics with molecules, materials, and living objects, *Langmuir* 36 (2020) 7158–7180.
- G. Roberts, *Langmuir–Blodgett films*, Plenum Press, New York, 1990.
- C.M. Knobler, Condensed monolayer phases at the air/water interface: Phase transitions and structures, *J. Phys.: Condens. Matter* 3 (1991) S17–S22.
- V.M. Kaganer, H. Möhwald, P. Dutta, Structure and phase transitions in Langmuir monolayers, *Rev. Mod. Phys.* 71 (1999) 779–818.
- J.C. Berg, *An Introduction to Interfaces and Colloids: The Bridge to Nanoscience*, World Scientific Publishers, Singapore, 2010.
- G. Wegner, Ultrathin films of polymers: Architecture, characterization and properties, *Thin Solid Films* 216 (1992) 105–116.
- G. Xu, Z. Bao, J.T. Groves, Langmuir–Blodgett films of regioregular poly(3-hexylthiophene) as field-effect transistors, *Langmuir* 16 (2000) 1834–1841.
- C.A. Olivati, V.C. Gonçalves, D.T. Balogh, Optically anisotropic and photoconducting Langmuir–Blodgett films of neat poly(3-hexylthiophene), *Thin Solid Films* 520 (2012) 2208–2210.
- L.-H. Chen, W.-P. Hsu, H.-W. Chan, Y.-L. Lee, Fabrication of P3HT/gold nanoparticle LB films by P3HT templating Langmuir monolayer, *Appl. Surf. Sci.* 320 (2014) 736–741.
- S. Oh, M. Yang, J. Bouffard, S. Hong, S.-J. Park, Air–liquid interfacial self-assembly of non-amphiphilic poly(3-hexylthiophene) homopolymers, *ACS Appl. Mater. Interfaces* 9 (2017) 12865–12871.
- I. Watanabe, K. Hong, F. Rubner, Langmuir–Blodgett manipulation of poly(3-alkylthiophenes), *Langmuir* 6 (1990) 1164–1172.
- J. Paloheimo, P. Kuivalainen, H. Stubb, E. Vuorimaa, P. Yli-Lahti, Molecular field-effect transistors using conducting polymer Langmuir–Blodgett films, *Appl. Phys. Lett.* 56 (1990) 1157–1159.
- A. Pawlicka, R.M. Faria, M. Yonashiro, S.V. Canevarolo Jr., O.N. Oliveira Jr., Effect of polymer molecular weight on Langmuir monolayers and the deposition of Langmuir–Blodgett films of poly(3-butylthiophene) and stearic acid, *Thin Solid Films* 244 (1994) 723–727.
- J.Z. Niu, G. Cheng, Z. Li, H. Wang, S. Lou, Z. Du, L.S. Li, Poly(3-dodecylthiophene) Langmuir–Blodgett films: Preparation and characterization, *Colloids Surf. A* 330 (2008) 62–66.
- E.A. da Silva, V.J.R. de Oliveira, M.L. Braunger, C.J.L. Constantino, C. de Almeida Olivati, Poly(3-octylthiophene)/stearic acid Langmuir and Langmuir–Blodgett films: Preparation and characterization, *Mater. Res.* 17 (2014) 1442–1448.
- E.A. da Silva, L. Caseli, C. de Almeida Olivati, Organization of polythiophenes at ultrathin films mixed with stearic acid investigated with polarization-modulation infrared reflection–absorption spectroscopy, *Colloids Surf. A* 529 (2017) 628–633.
- J.K. Bal, S. Kundu, S. Hazra, Hydrophobic to hydrophilic transition of HF-treated Si surface during Langmuir–Blodgett film deposition, *Chem. Phys. Lett.* 500 (2010) 90–95.
- P. Chatterjee, S. Hazra, The hydrophilic/hydrophobic nature of a Cl-terminated Si surface, *Soft Matter* 9 (2013) 9799–9806.
- L.J. Parratt, Surface studies of solids by total reflection of X-rays, *Phys. Rev.* 95 (1954) 359–369.
- A. Gibaud, S. Hazra, X-ray reflectivity and diffuse scattering, *Curr. Sci.* 78 (2000) 1467–1477.
- A. Gibaud, G. Vignaud, X-ray and Neutron Reflectivity: Principles and Applications, Springer, Berlin, 2009, pp. 85–131.
- P. Chatterjee, S. Hazra, H. Amenitsch, Substrate and drying effect in shape and ordering of micelles inside CTAB–silica mesostructured films, *Soft Matter* 8 (2012) 2956–2964.
- R.P. Giri, A. Chakrabarti, M.K. Mukhopadhyay, Cholesterol-induced structural changes in saturated phospholipid model membranes revealed through X-ray scattering technique, *J. Phys. Chem. B* 121 (2017) 4081–4090.
- J.K. Bal, S. Hazra, Interfacial role in room-temperature diffusion of Au into Si substrates, *Phys. Rev. B* 75 (2007) 205411.
- J.K. Bal, S. Hazra, Time-evolution growth of Ag nanolayers on differently-passivated Si(001) surfaces, *Phys. Rev. B* 79 (2009) 155412.
- P. Chatterjee, S. Hazra, Time evolution of a Cl-terminated Si surface at ambient conditions, *J. Phys. Chem. C* 118 (2014) 11350–11356.
- S. Sinha, M. Mukherjee, Thickness dependent electronic structure and morphology of rubrene thin films on metal, semiconductor, and dielectric substrates, *J. Appl. Phys.* 114 (2013) 083709.
- S. Mandal, M. Mukherjee, S. Hazra, Evolution of electronic structures of polar phthalocyanine–substrate interfaces, *ACS Appl. Mater. Interfaces* 12 (2020) 45564–45573.
- I. Horcas, R. Fernández, J.M. Gómez-Rodríguez, J. Colchero, J. Gómez-Herrero, A.M. Baro, WSXM: A software for scanning probe microscopy and a tool for nanotechnology, *Rev. Sci. Instrum.* 78 (2007) 013705.
- R.B. Corey, L. Pauling, Molecular models of amino acids, peptides, and proteins, *Rev. Sci. Instrum.* 24 (1953) 621–627.
- W.L. Koltun, Precision space-filling atomic models, *Biopolymers* 3 (1965) 665–679.
- Y. Xu, Y. Liu, J. Wu, D. Zhu, Preparation and electrical conductivity of Langmuir–Blodgett films of poly(3-alkylthiophenes), *J. Appl. Polym. Sci.* 69 (1998) 1–6.
- J.T. Davies, E.K. Rideal, *Interfacial Phenomena*, Academic Press, New York, 1963.

- [57] M.D. Phan, O.I. Korotych, N.G. Brady, M.M. Davis, S.K. Satija, J.F. Ankner, B.D. Bruce, X-ray and neutron reflectivity studies of styrene-maleic acid copolymer interactions with galactolipid-containing monolayers, *Langmuir* 36 (2020) 3970–3980.
- [58] G.L. Gaines Jr., Thermodynamic relationships for mixed insoluble monolayers, *J. Colloid Interface Sci.* 21 (1966) 315–319.
- [59] I. Ahmed, L. Dildar, A. Haque, P. Patra, M. Mukhopadhyay, S. Hazra, M. Kulkarni, S. Thomas, J.R. Plaisier, S.B. Dutta, J.K. Bal, Chitosan–fatty acid interaction mediated growth of Langmuir monolayer and Langmuir–Blodgett films, *J. Colloid Interface Sci.* 514 (2018) 433–442.
- [60] P. Mélinon, P. Kéghélian, B. Prével, A. Perez, G. Guiraud, J. LeBrusq, J. Lermé, M. Pellarin, M. Broyer, Nanostructured silicon films obtained by neutral cluster depositions, *J. Chem. Phys.* 107 (1997) 10278–10287.
- [61] G. Hazell, A.P. Gee, T. Arnold, K.J. Edler, S.E. Lewis, Langmuir monolayers composed of single and double tail sulfobetaine lipids, *J. Colloid Interface Sci.* 474 (2016) 190–198.
- [62] R.A. Campbell, Y. Saaka, Y. Shao, Y. Gerelli, R. Cubitt, E. Nazaruk, D. Matyszevska, M.J. Lawrence, Structure of surfactant and phospholipid monolayers at the air/water interface modeled from neutron reflectivity data, *J. Colloid Interface Sci.* 531 (2018) 98–108.